Supporting Information

Improved resistive switching performance and realized electric control of exchange bias in a NiO/HfO_2 bilayer structure

Yu Lu,[1] Yuan Yuan,[1] Ruobai Liu,[1] Tianyu Liu,[1] Jiarui Chen,[1] Lujun Wei,[2] Di Wu,[1] Wei Zhang,[1] Biao You,[1] Jun Du[,1,3]*

[1]National Laboratory of Solid State Microstructures and Department of Physics, Nanjing University, Nanjing 210093, P. R. China

[2]School of Science, Nanjing University of Posts and Telecommunications, Nanjing 210046, P. R. China

[3]Collaborative Innovation Center of Advanced Microstructures, Nanjing 210093, P. R. China

*Email: jdu@nju.edu.cn (J. Du).

S1. Cross-sectional SEM image and optical micrograph for the Pt/Co/NiO/HfO_2/ Pt device

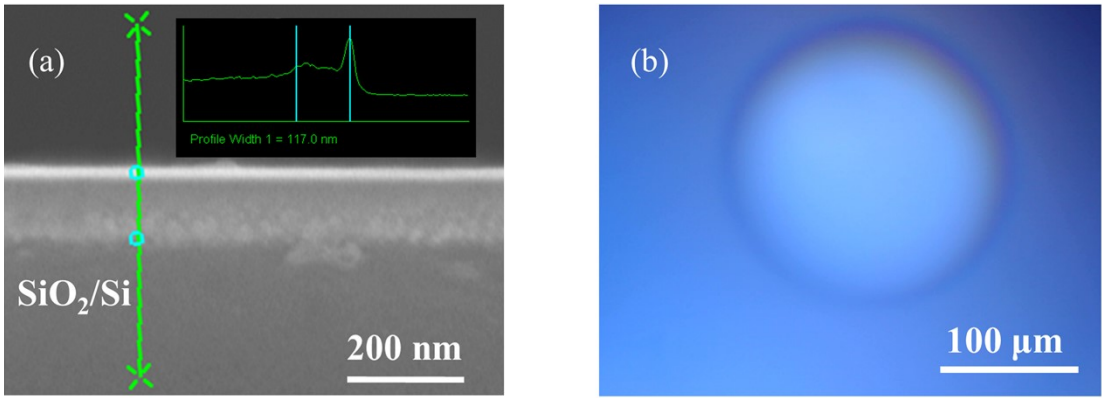

Figure S1. (a) Cross-sectional SEM image for the Pt/Co/NiO/HfO_2/Pt film sample and (b) optical micrograph taken in a top electrode area for the Pt/Co/NiO/HfO_2/Pt device. The total thickness is measured to be about 117 nm in (a) and the diameter of the top electrode is measured be about 210 nm in (b).

S2. *I-V* characteristics and RS performance for the Pt/HfO_2/Pt device

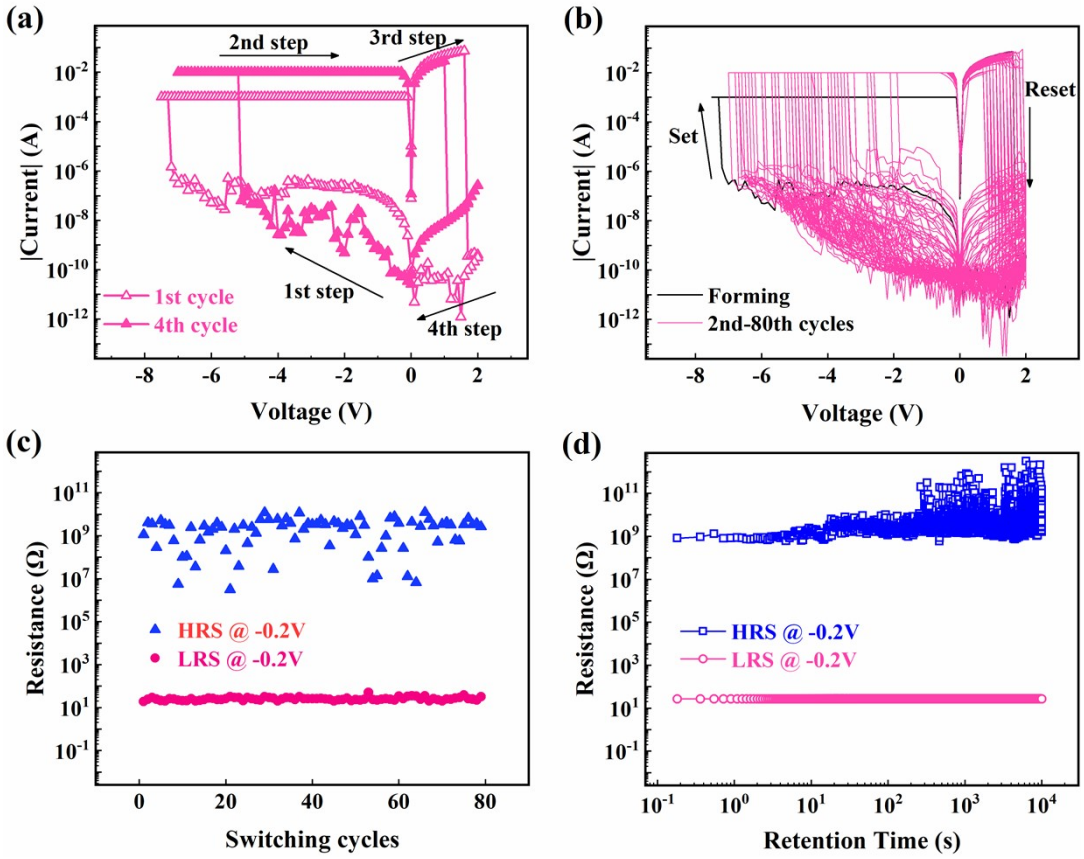

Figure S2. (a) Comparison of the first and fourth *I-V* curve of the Pt/HfO_2/Pt device. (b) Consecutively recorded *I-V* curves (80 cycles) for the same device in (a). (c) The cycle number and (d) time dependences of the same device's resistance at HRS and LRS under an applied voltage of -0.2 V.

S3. *I-V* curve measured with applying high voltage for the Pt/NiO/Pt device

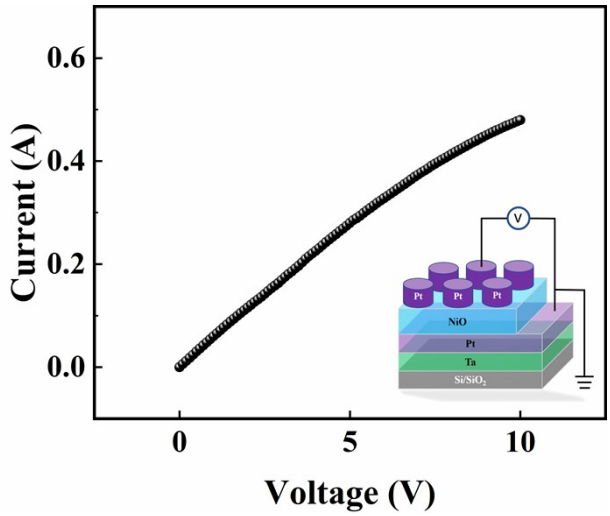

Figure S3. The *I-V* curve for the Pt/NiO/Pt device without applying a compliance current. The inset shows the schematic diagram for the device's structure and *I-V* measurement configuration.

S4. AC switching transition behavior in the Pt/Co/NiO/HfO_2/Pt device

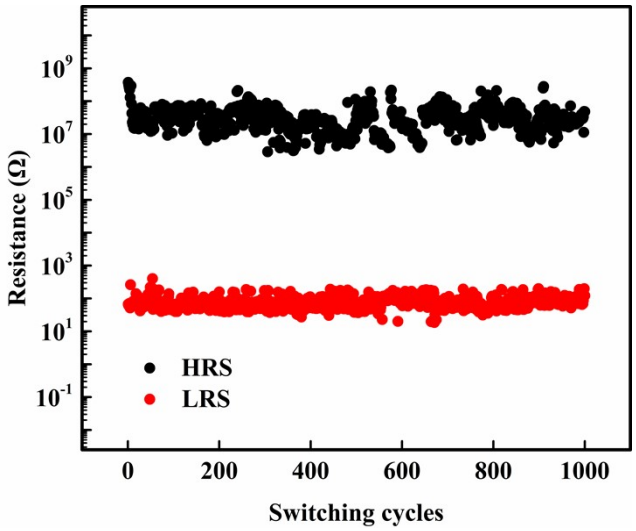

Figure S4. The switching cycle number dependences of the Pt/Co/NiO/HfO_2/Pt device's resistances at HRS (black) and LRS (red) measured by pulsed voltage. More than 1000 switching cycles were obtained under alternate set (-5 V, 50 ms) and reset (2 V, 50 ms) voltage pulses, and the resistance at HRS and LRS were recorded by another voltage pulse of (-0.2 V, 50 ms) with much smaller amplitude.

S5. RS performance checking at 85℃ for the Pt/Co/NiO/HfO_2/Pt device

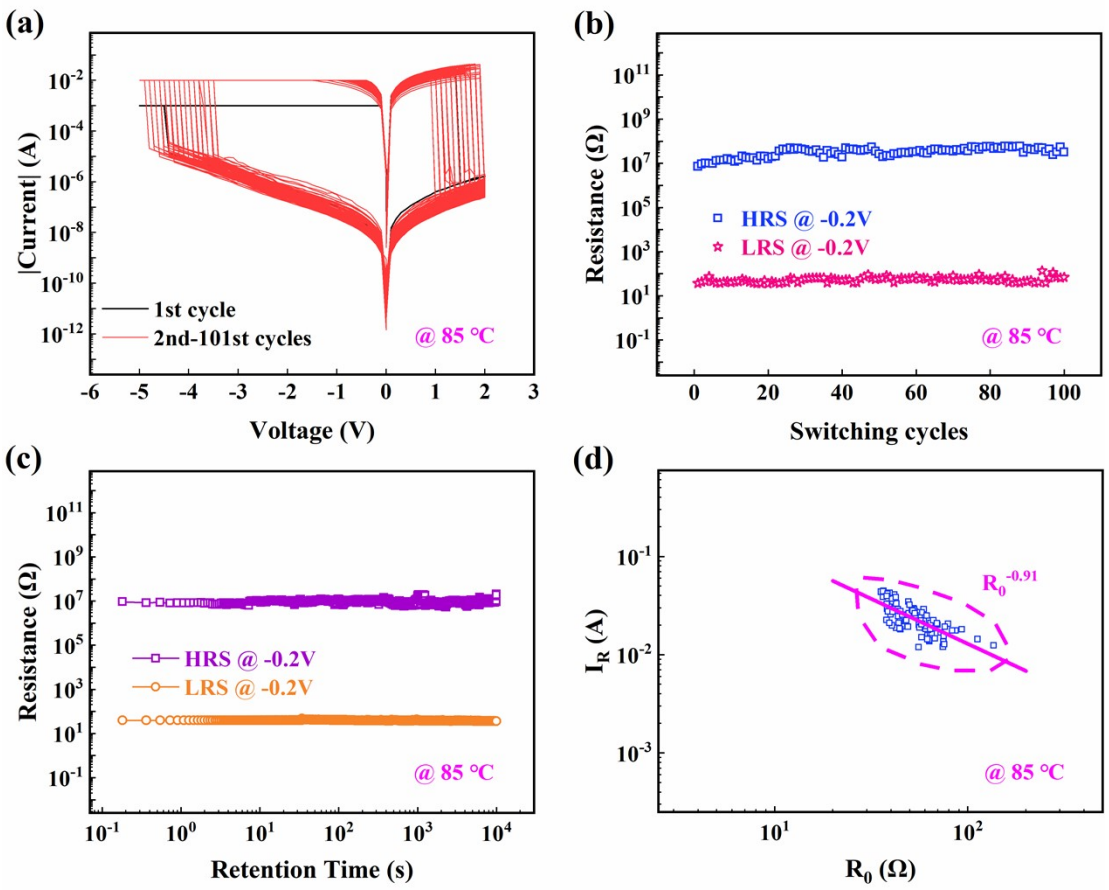

Figure S5. (a) Consecutively recorded *I-V* curves (101 cycles), (b) cycle number and (c) time dependences of the resistance at HRS and LRS under an applied voltage of -0.2 V, (d) $I_R \sim R_0$ plotted in log-log scale measured at 85 ℃ for the Pt/Co/NiO/HfO_2/Pt device.

S6. Device-to-device variability analysis

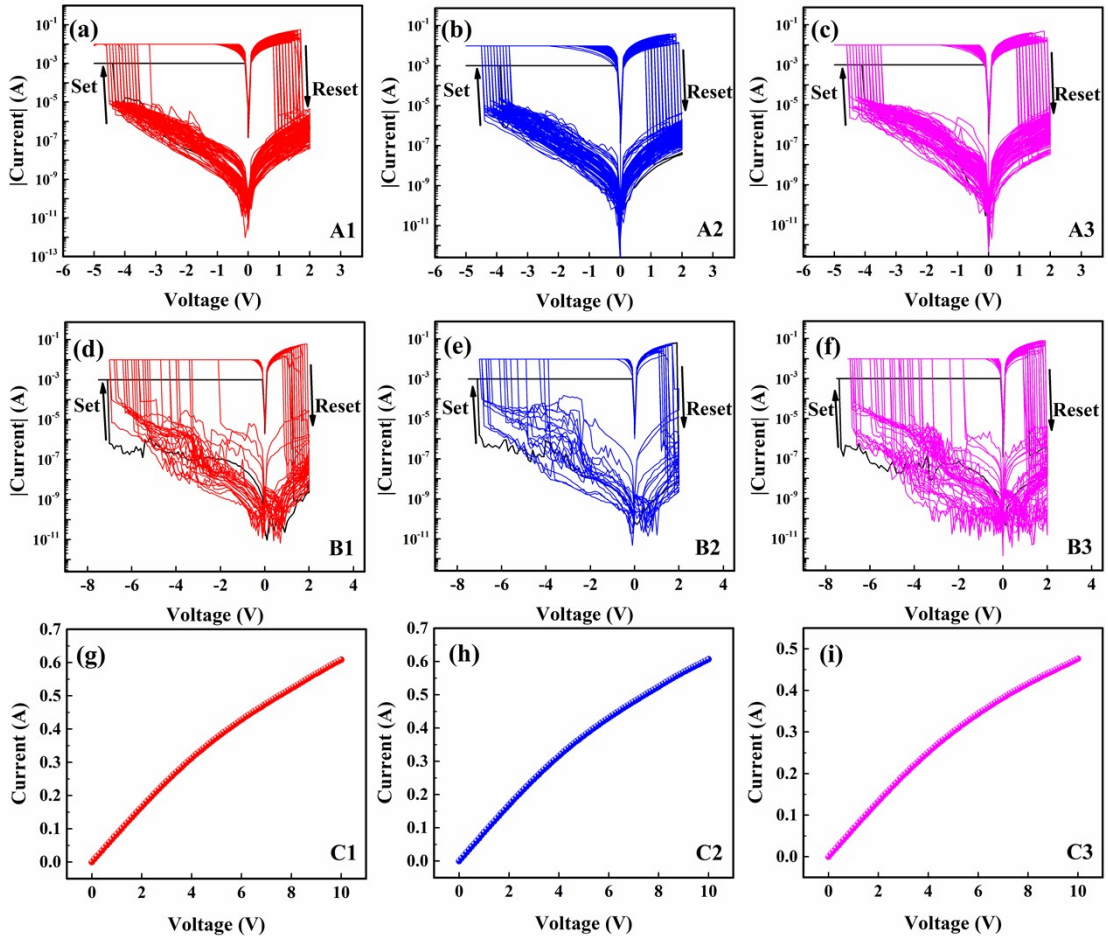

Figure S6. *I-V* curves for the devices of (a)-(c) Pt/Co/NiO/HfO_2/Pt (series A: A1-A3), (d)-(f) Pt/HfO_2/Pt (series B: B1-B3) and (g)-(i) Pt/NiO/Pt (series C: C1-C3).

S7. Investigation of conduction mechanism at positive bias region for the Pt/Co/NiO/HfO_2/Pt device

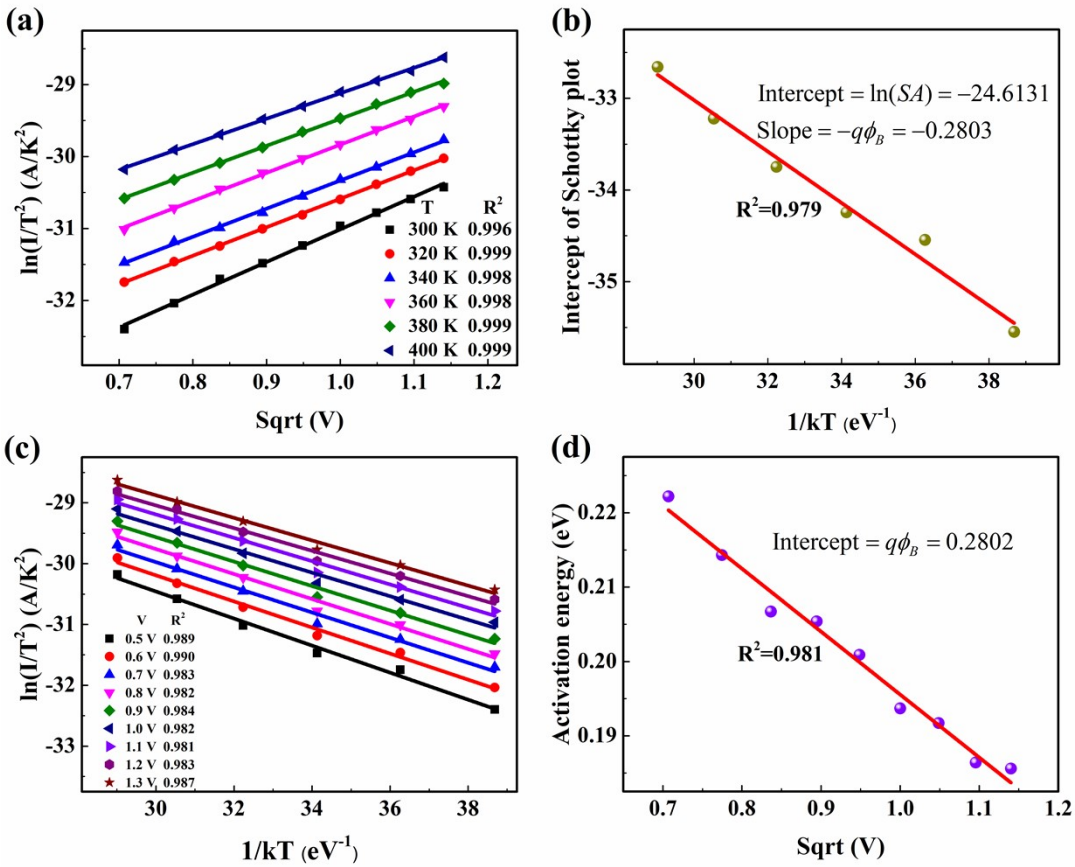

Figure S7. (a) The Schottky plots in the low positive voltage region from 0.5 V to 1.3 V at various temperatures, (b) the intercepts of each Schottky plot in (a) versus 1/kT, (c) the Arrhenius plots at various voltages, (d) the activation energy versus Sqrt (V) for the Pt/Co/NiO/HfO_2/Pt device. All the solid lines denote the linear fitting results. All the R^2 values denote the coefficients of determination.

S8. *R-T* curve measurements for different RS devices at LRS

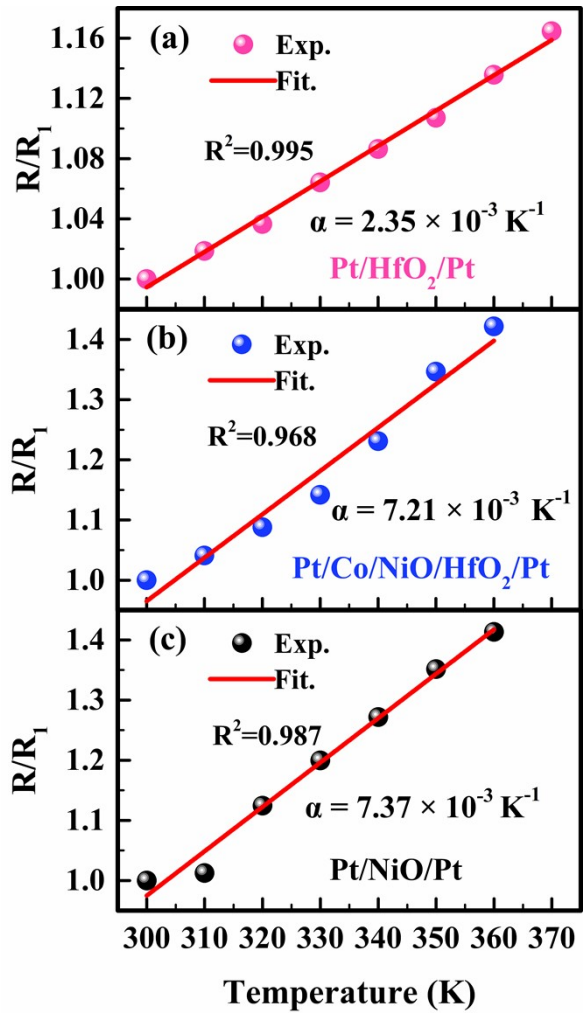

Figure S8. (a) Temperature dependences of the normalized resistance (R/R_1) measured at LRS for the devices of (a) Pt/HfO_2/Pt, (b) Pt/Co/NiO/HfO_2/Pt and (c) Pt/NiO/Pt. The red solid lines denote the linear fitting results. All the R^2 values denote the coefficients of determination.

S9. Comparison of energy band diagrams under positive and negative biased voltages for the Pt/Co/NiO/HfO_2/Pt device

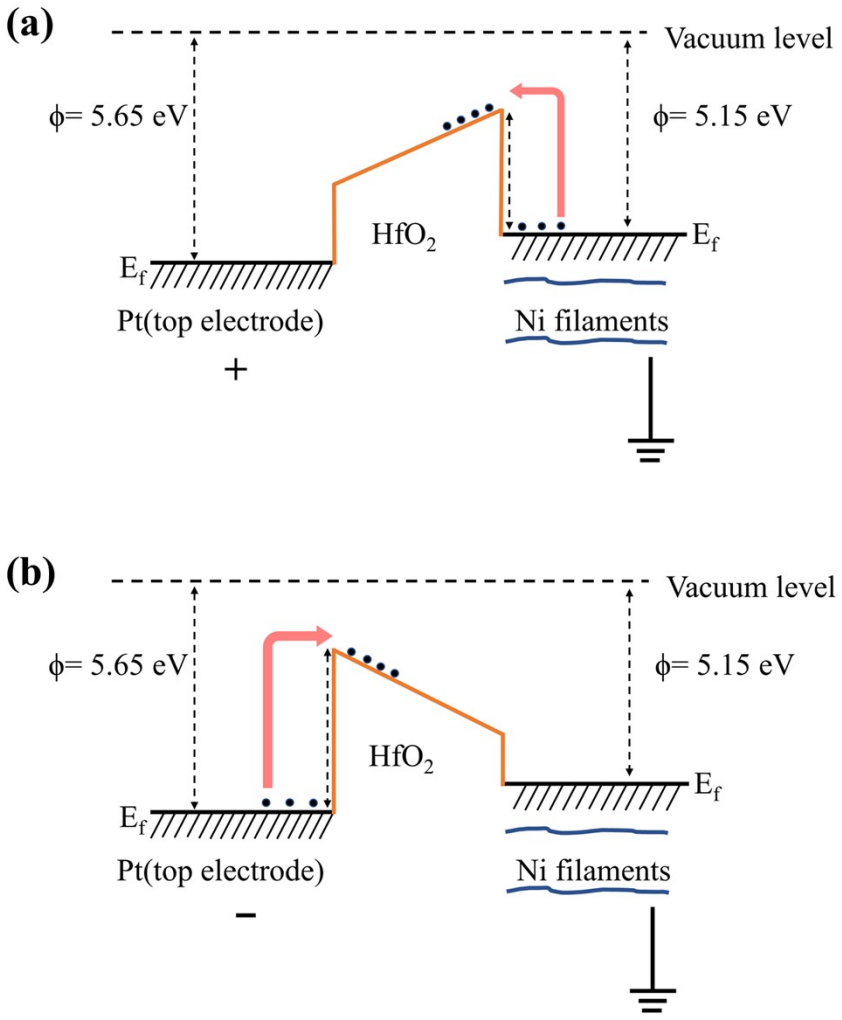

Figure S9. Energy band diagrams under (a) positive and (b) large negative biased voltages for the Pt/Co/NiO/HfO_2/Pt device.

S10. Scaling behavior analyses on other parameters

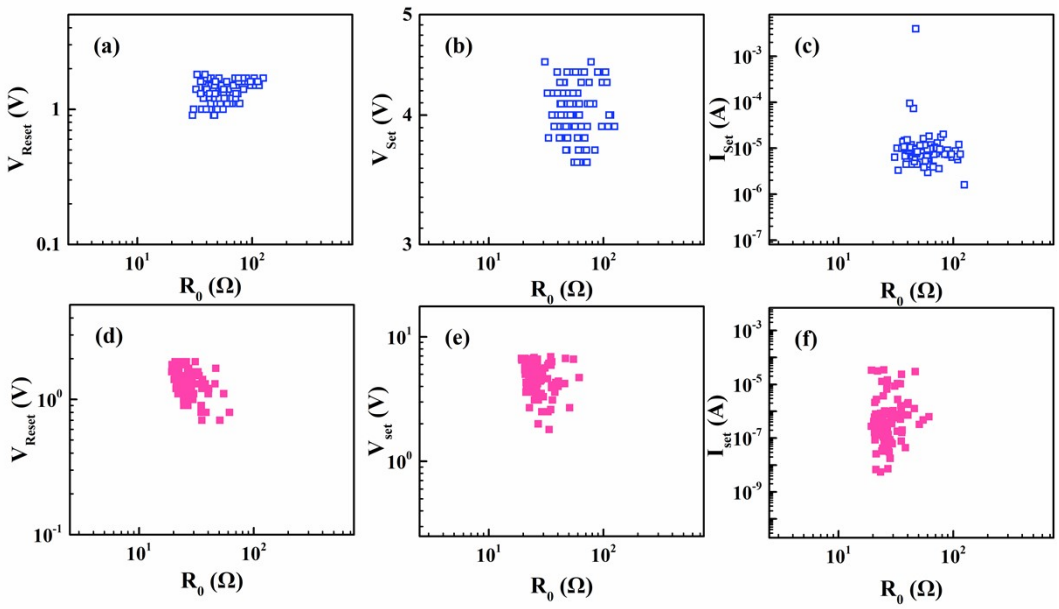

Figure S10. (a) V_{Reset}, (b) V_{Set} and (c) I_{Set} against R_0 for the Pt/Co/NiO/HfO_2/Pt device; (d) V_{Reset}, (e) V_{Set} and (f) I_{Set} against R_0 for the Pt/HfO_2/Pt device.

S11. Electric control of EB in the Pt/Co/NiO/HfO_2/Pt/ITO device

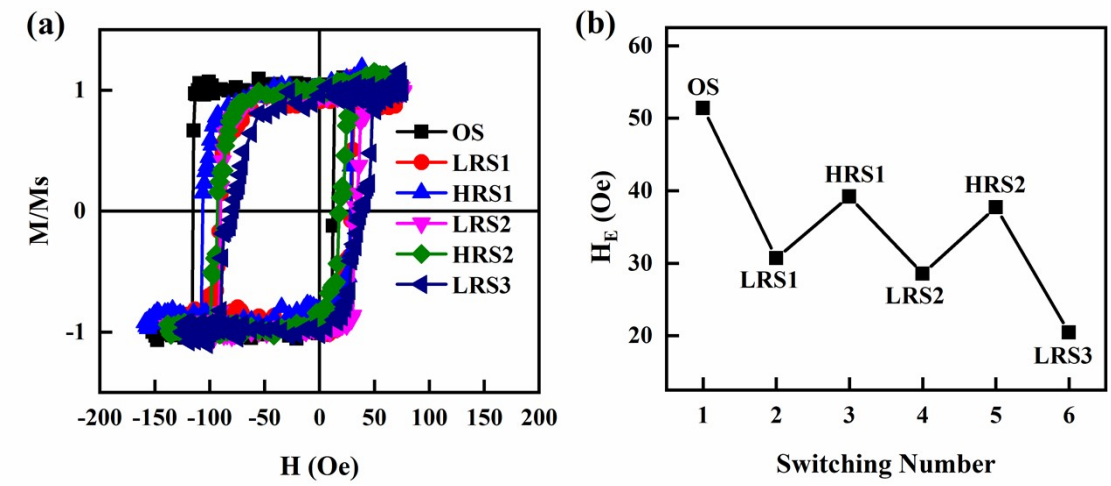

Figure S11. (a) *M-H* loops measured at OS, the first LRS (LRS1), the first HRS (HRS1), the second LRS (LRS2), the second HRS (HRS2), the third LRS (LRS3) and (b) H_E against the cycle number in the initial three cycles for the Pt/Co/NiO/HfO_2/Pt/ITO device.

S12. Influence of oxygen concentration in the NiO layer on the EB for the Co/NiO bilayer

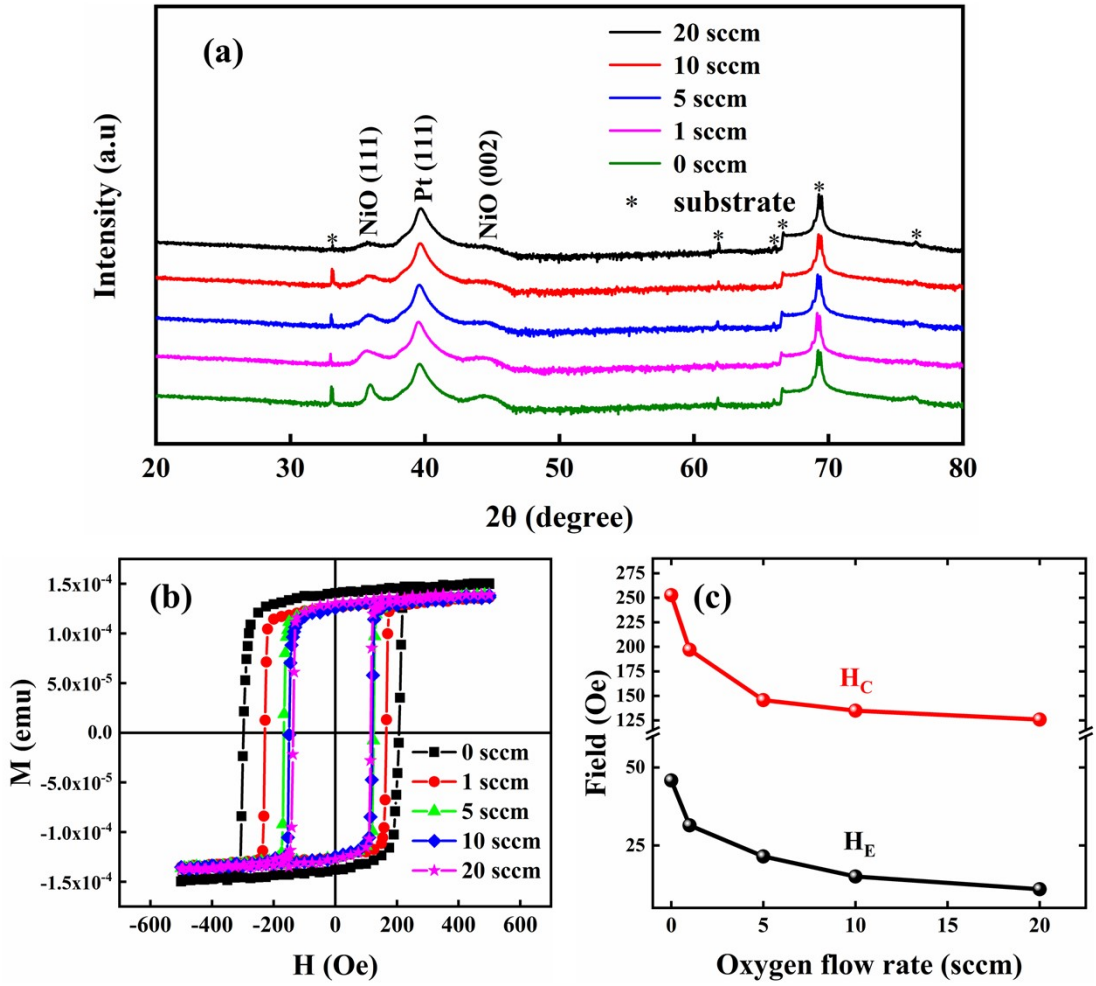

Figure S12. (a) XRD patterns for the Si/SiO_2/Ta(5)/Pt(30)/NiO(35)/Co(6)/Al(5) film samples with various oxygen flow rates (0, 1, 5, 10 and 20 sccm) during deposition of the NiO layers. (b) *M*-*H* loops and (c) the oxygen flow rate dependences of H_C and H_E for the RS devices fabricated using the corresponding films indicated in (a).